ORIGINAL ARTICLE

lajss.org
Latin American Journal of Solids and Structures

www.lajss.org

Numerical Analysis of the Dynamic Tensile Behavior of Cement-Based Materials using a Gravity-Driven Hopkinson Tension Bar

Ammar Babiker[a]*, Ebtihaj Abu-Elgasim[a], Mashair Mohammed[a]

[a]School of Civil Engineering, College of Engineering, Sudan University of Science and Technology, P.O. Box 72, Eastern Daim, Khartoum, Sudan. E-mail: ammar.babiker@sustech.edu, ebtihaj.gasim@sustech.edu, mashair.ama@sustech.edu

*Corresponding author

https://doi.org/10.1590/1679-78257483

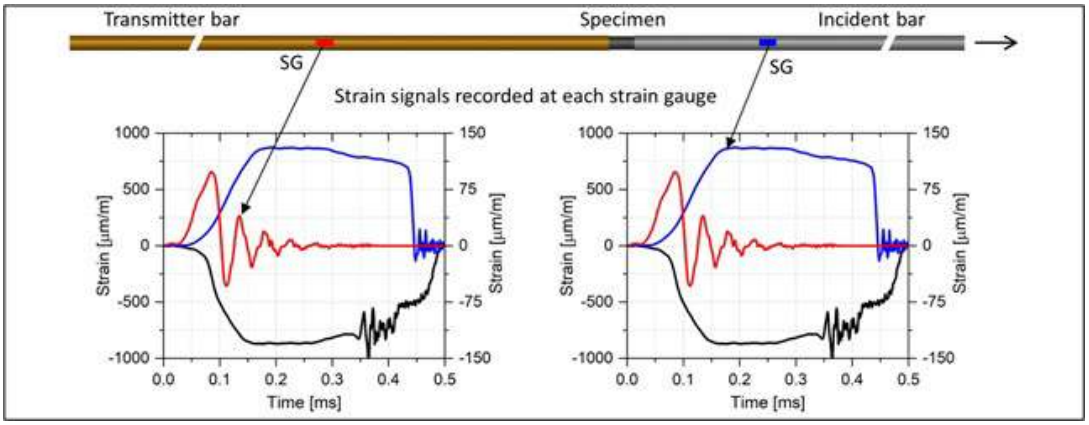
Abstract

Dynamic characterization of cement-based composites is crucial for understanding material behavior. When exposed to highly dynamic loading conditions, the strain-rate dependence of material causes the material response to differ significantly from that under quasi-static loading conditions. In this paper, a numerical investigation on the dynamic tensile behavior of cement-based materials. A gravitational split Hopkinson tension bar was used to characterize the dynamic tensile behavior of cement-based at high strain-rates. The commercial finite element software LS-Dyna is adopted to conduct the computations. The material specifications of cement-based are characterized by the Karagozian & Case (K&C) concrete model that accounts for shear dilation, strain-rate dependence, and strain softening. The model accuracy is verified with available experimental results in the form of strain signals, strain-rates, and tensile strengths. It was found that the results computed with the automatic generation version of K&C are slightly different from the experimental ones. Therefore, to achieve better agreement, the model was extended by calibrating a few parameters of the K&C material formulation. Finally, the simulation predictions were found to represent the experimental results with good agreement.

Keywords

Split Hopkinson bar, Dynamic tensile strength, Strain-rate, Cement-based, K&C, LS-Dyna

Graphical Abstract



Received: January 26, 2023. In revised form: July 15, 2023. Accepted: July 17, 2023. Available online: July 26, 2023.
https://doi.org/10.1590/1679-78257483

Latin American Journal of Solids and Structures. ISSN 1679-7825. Copyright © 2023. This is an Open Access article distributed under the terms of the Creative Commons Attribution License, which permits unrestricted use, distribution, and reproduction in any medium, provided the original work is properly cited.

1 INTRODUCTION

Understanding the behavior of cementitious materials such as concrete at various loading rates is essential for the adequate design of structural members subjected to high loading rates. Today, the design strategy is built on computational analysis using detailed material models capable of representing dynamic effects. The split Hopkinson tension bar (SHTB) is a modified version of the original split Hopkinson bar configuration (SHB) developed by (H. Kolsky 1949) and is a prevalent method for investigating the tensile dynamic material behavior at high strain rates of 10 to 10^4 s^{-1} (Cooper and Campbell 1967; Nicholas 1981). In more than three decades of research, the dynamic behavior of concrete and cement-based materials has been examined extensively, but main efforts have focused on the compressive behavior of concrete and cement-based composites, for which more data are available, and less on their tensile behavior (Levi-Hevroni et al. 2018). This could be related to the measurement simplicity of materials under compression than that under tension.

Cementitious materials are generally classified as strain-rate sensitive materials. With increasing strain-rate, both compressive and tensile strengths increase. This phenomenon is more pronounced when the strain-rate exceeds the transition strain-rate (about 102 s^{-1} in compression and 100−101 s^{-1} in tension) (Li and Xu 2009; Ross, Thompson, and Tedesco 1989; Wang, Zhang, and Quek 2012).

A number of experimental and numerical investigations of dynamic tensile behavior have been reported in the literature by using different types of materials, e.g., concrete, rocks, cement-based, quasi-ductile, and strain-hardening cement-based (Cadoni and Forni 2016; Chen, Wu, and Zhou 2014; Curosu et al. 2017; Curosu, Mechtcherine, and Millon 2016; Hao, Zhang, and Hao 2011; Heravi, Curosu, and Mechtcherine 2020; Levi-Hevroni et al. 2018; Ross, Thompson, and Tedesco 1989; Staab and Gilat 1991). In the present research, finite-element (FE) simulations are performed using a strain-rate sensitive material model in LS-Dyna (LST- LIVERMORE SOFTWARE TECHNOLOGY, 2021) to study the dynamic tensile behavior of cement-based materials in an SHTB test. Shear dilation is also included in the material model adopted in these models. In numerical simulations, two different versions of concrete damage material models are used, i.e., the original and the modified or calibrated version. The results from the original and the modified models are compared, and the contribution of the material modifications to the dynamic tensile strength is analyzed.

2 FUNDAMENTAL OF SHTB

The gravitational SHTB is a type of experimental apparatus used to study the dynamic behavior of materials under high strain-rate loading. It is a modified version of the conventional split Hopkinson pressure bar configuration developed by (H. Kolsky 1949), which is a testing machine used for characterizing the dynamic mechanical properties of materials exposed to tensile loading. The schematic illustration of the SHTB setup is presented in Figure 1.

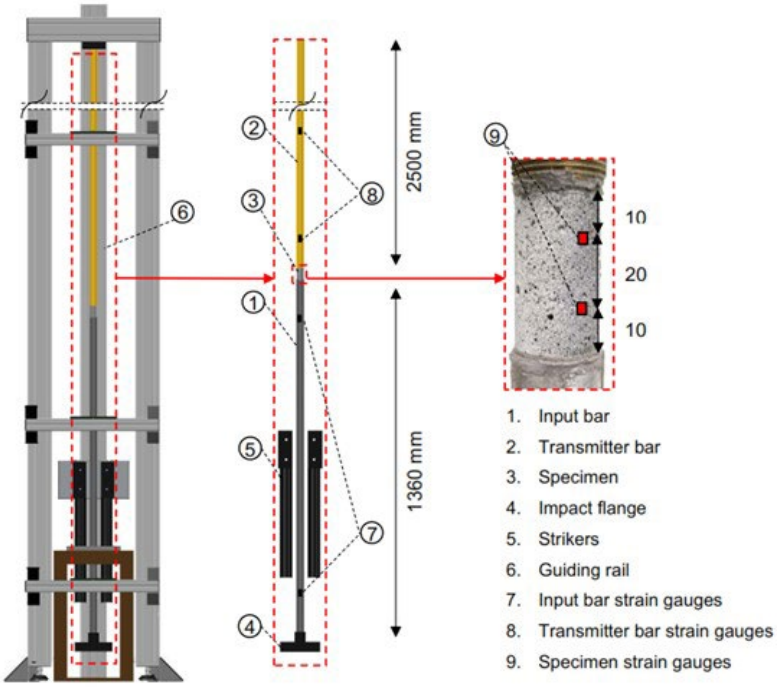


Figure 1 Gravitational Hopkinson bar apparatus used in (Heravi, Curosu, and Mechtcherine 2020).

The SHTB system consists of an incident (input) bar, a transmitter (output) bar, and a specimen sandwiched between the two bars. In the SHTB experiment, a steel striker is dropped from a variable height onto the impact flange of the incident bar. This produces a tensile stress wave that propagates upwards through the incident bar. The tensile stress wave is partially reflected as it reaches the interface between the input bar and the specimen. A part of the wave returns towards the impact flange as a compressive wave, while the rest is transmitted through the sample and into the output bar. This process causes elastic and distortion in the sample. The ratio between the transmitted and reflected strain waves in the SHTB experiment depends on the mechanical impedance of the involved materials. In the SHTB system, strain gauges are typically mounted on both the incident and transmitter bars at specific locations in order to measure the deformation of the bars as the stress propagates through them.

3 SHTB THEORY

According to the Hopkinson bar's one-dimensional wave propagation theory (H. Kolsky 1949), when the specimen rod reaches stress equilibrium. Using the incident, reflected, and transmitted waves (ε_i, ε_r, ε_t), the forces at the interface between the input bar and the sample and between the output bar and the sample are calculated based on Eqs. (1) and (2).

$$F_i(t) = A_i E_i(\varepsilon_i(t) + \varepsilon_r(t)) \tag{1}$$

$$F_i(t) = A_i E_i(\varepsilon_i(t) + \varepsilon_r(t)) \tag{2}$$

where E_i and E_t are Young's modulus of the input and output bars material, respectively, A_i and A_t are the cross-sectional area in the incident and transmitter bars, respectively. The displacement at the ends of the specimen can be delivered with the help of Eqs. (3) and (4).

$$\delta_i(t) = C_i \int (\varepsilon_i(t) - \varepsilon_r(t))dt \tag{3}$$

$$\delta_t(t) = C_t \int (\varepsilon_t(t))dt \tag{4}$$

The velocities at the end of the specimens are deduced using Eqs. (5) and (6), in which C_i and C_t are elastic wave speeds of the incident and transmitter bars, respectively.

$$V_i(t) = C_i(\varepsilon_i(t) - \varepsilon_r(t)) \tag{5}$$

$$V_t(t) = C_t(\varepsilon_t(t)) \tag{6}$$

It is important to note that the elastic wave speed C will depend on the properties of the medium through which the wave is traveling. Calculation of incident and transmitter bar elastic speeds is done using the strain signals of the attached strain gauges, see Figure 2. Knowing the distance between the attached strain gauges and the required time for the wave to travel between them and relating the distance and the time, the wave speed can be determined according to Eq. (7), where Δx and Δt are the distance and time between respective signals.

$$C = \frac{\Delta x}{\Delta t} \tag{7}$$

For the derivation of the dynamic elastic modulus, the elastic wave velocity is used; see Eq. (8), which ρ defines material density.

$$E_{\text{dyn}} = C^2 \rho \tag{8}$$

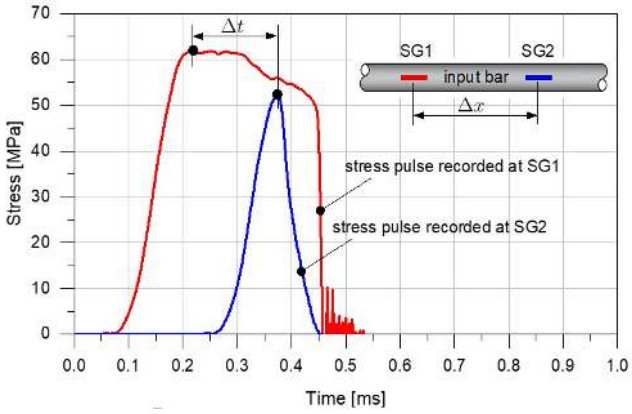


Figure 2 Example of stress-time history of the incident bar.

3.1 Calculation of Dynamic Tensile Stress

3.1.1 Indirect Method

According to the Hopkinson bar's wave theory discussed in Section 3, the stress, strain, and strain-rate of the specimens are derived using Eqs. (9), (10), and (11), where A_s and L_s define the cross-sectional area and the length of the sample, respectively.

$$\sigma_s = \frac{F_i(t) + f_t(t)}{2A_s} \tag{9}$$

$$\varepsilon_s = \frac{\delta_i(t) - \delta_t(t)}{L_s} \tag{10}$$

$$\dot{\varepsilon}_s = \frac{V_i(t) - V_t(t)}{L_s} \tag{11}$$

3.1.2 Direct Method

Unlike the previous technique, this method uses the longitudinal transmitted tensile stress wave in the specimen to compute the dynamic tensile stress. Therefore, herein method, the incident ε_i, reflected ε_r, and transmitted ε_t pulses are not involved.

4 SIMULATION OF SHTB EXPERIMENT

The simulations of the SHTB test in this investigation were conducted with a similar set-up as that reported by Heravi et al. (Heravi, Curosu, and Mechtcherine 2020), in which an experimental investigation on gravitational SHTB testing for various composites is presented. It is important to note that this work only considered the normal strength cement-based matrix. The computations were performed using LS-Dyna software suitable for modeling dynamic problems with wave propagation. The following covers the simulation details of SHTB experiments according to Heravi et al. (Heravi, Curosu, and Mechtcherine 2020).

4.1 Geometry and Discretization

In the SHTB system used in this study, the dimensions are given with a 22.2 mm diameter for the specimen and a length of 40 mm. The bars have a constant diameter of 24 mm and a length of 1360 mm for the incident bar and 2500 mm for the transmitter bar, see Figure 1. The incident bar is made from aluminum, whereas the transmitter bar is from brass. The sample is attached to the incident and transmitter bars with a 24 mm diameter epoxy resin adhesive.

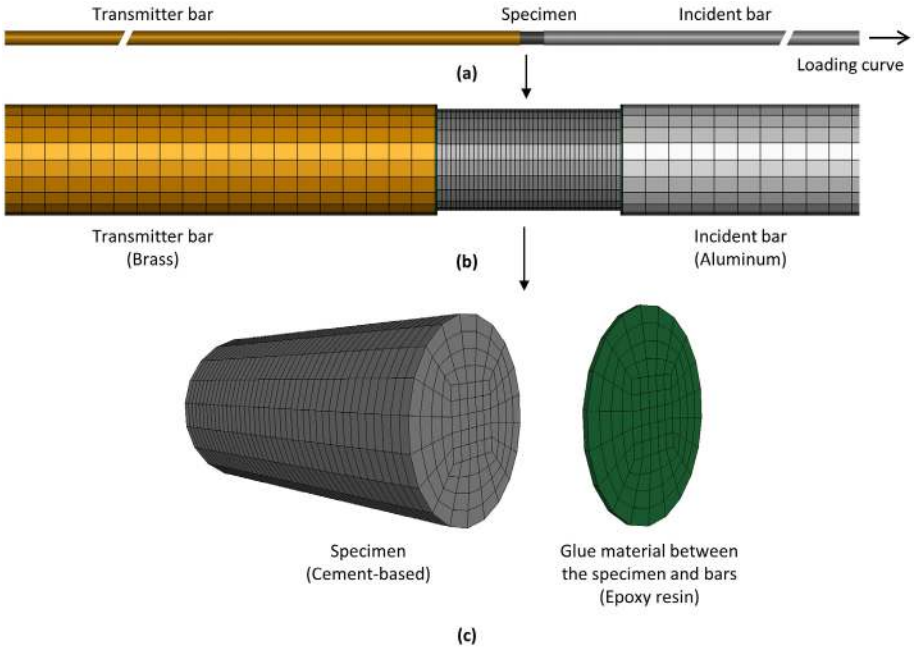


Figure 3 Finite element model of SHTB experiment: (a) complete FE model, (b) discretization of specimen and bars, and (c) discretization of specimen and glue materials.

To minimize the computational time, Eight-node Lagrangian solid elements are adopted to model all parts of the SHTB system with the default formulation. The elements of the specimen and the incident and transmitter bars have an average mesh size of about 5 mm. The model discretization is presented in Figure 3. Furthermore, an outline of the material types, number of nodes, and elements are presented in Table 1. The experimentally recorded input wave is shown in Figure 4. This impact velocity is used as a loading curve, and it is applied to the free-end surface nodes set of the incident bar utilizing the *INITIAL_VELOCITY_GENERATION keyword in LS-Dyna. To prevent the transmitter bar from any movements, its free surface node set is constrained in all directions.

Table 1 Numerical model details.

Phase	Material	Length [mm]	Diameter [mm]	Elements	Nodes
Specimen	Cement-based	40	22.5	4200	4756
Incident bar	Aluminum	1360	24	28560	31668
Transmitter bar	Brass	2500	24	52500	58116
Glue	Epoxy resin	1	24	210	464

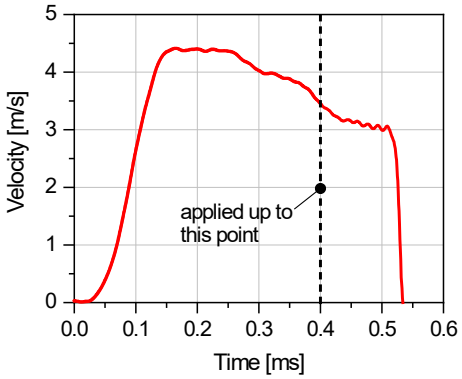


Figure 4 Loading function.

4.2 Contact Algorithms

An appropriate contact algorithm has to be defined between each part of the SHTB system to prevent any interpenetration. In this work, a contact algorithm *TIED_SURFACE_TO_SURAFCE was adopted to achieve a perfect

contact between the glue material and the specimen. The glue materials have their interfacing nodes set in common with the input and transmitter bars; see Figure 3. This allows for modeling a perfect bond using a frictionless *AUTOMATIC SURFACE TO SURFACE contact algorithm of LS-Dyna.

4.3 Constitutive Material Model

A Constitutive material model is a mathematical model used to describe the behavior of a particular material under different loading scenarios. There are many different types of constitutive material models, each suited to different types of materials and loading conditions.

4.3.1 Material Model for Concrete

For concrete and cement-based composites subjected to high strain-rates, LS-Dyna explicit software provides a variety of material models. In this paper, the Karagozian & Case concrete damage model was employed to simulate and analyze the performance of cement-based materials.

One of the most used material models for cementitious materials, the Karagozian & Case (K&C) concrete damage model (*MAT_072R3), was developed and enhanced by (Malvar et al. 1995, 1996; Malvar, Crawford, and Morrill 2000) and implanted into the LS-Dyna material library. The K&C model is an advanced elastic-plastic material formulation that uses three failure surfaces to describe the formulation behavior. According to Figure 5, the failure surfaces are the initial σ_y, maximum σ_m, and residual σ_r failure surfaces.

As soon as the stress reaches the initial failure surface σ_y, the current stress σ can be derived using the linear interpolation between the initial and the maximum failure surfaces, see Eq. (12).

$$\sigma = \eta(\sigma_m - \sigma_y) + \sigma_y \tag{12}$$

Similarly, following the maximum failure surface σ_m, the current stress σ can be determined by applying Eq. (13).

$$\sigma = \eta(\sigma_m - \sigma_r) + \sigma_r \tag{13}$$

The parameter η defines the effective plastic stain damage function ranging from zero to one. This function depends on the accumulative effective plastic strain λ, see Figure 7 (a).

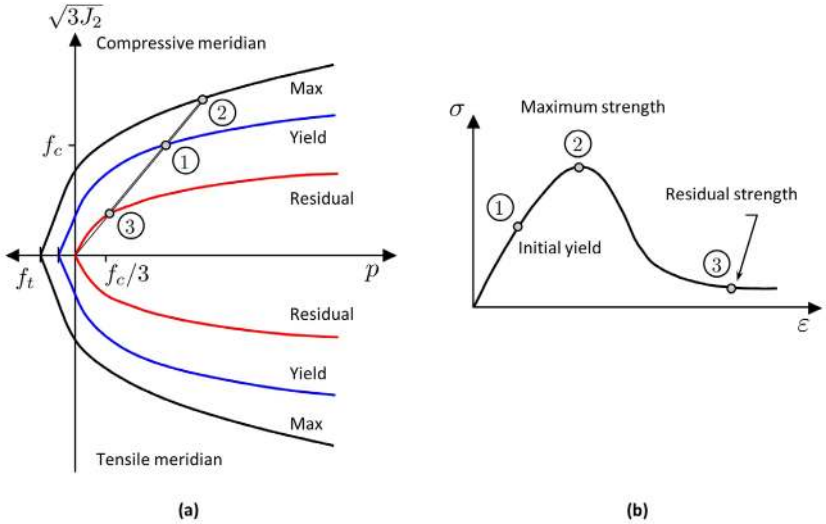


Figure 5 Concrete damage model: (a) yield surfaces, and (b) corresponding softening behavior.

The three failure surfaces of the K&C model are given in Eqs. (14) - (16), where p defines the hydrostatic pressure, a_{0y}, a_{1y}, and a_{2y} are the initial failure surface parameters, a_0, a_1, and a_2 are the maximum failure surface parameters, and a_{1f}, a_{2f} are the residual failure surface parameters. These parameters are responsible for defining the shape of each surface.

$$\sigma_y = a_{0y} \frac{p}{a_{1y} + a_{2y} p} \tag{14}$$

$$\sigma_m = a_0 \frac{p}{a_1 + a_2 p} \tag{15}$$

$$\sigma_r = \frac{p}{a_{1f} + a_{2f} p} \tag{16}$$

In general, the stress-strain behavior of concrete is complex and affected by multiple physical mechanisms, such as internal cracking, and it is also affected by the triaxial stress state. To account for such complexity, the K&C material model is provided with a damage function, see Figure 7(a). The damage function is given by Eqs. (17) and (18), where $d\bar{\varepsilon}^p$ is the effective plastic strain increment given by Eq. (19). b_1 and b_2 are damage scaling for the cases of uniaxial compression and tension, respectively.

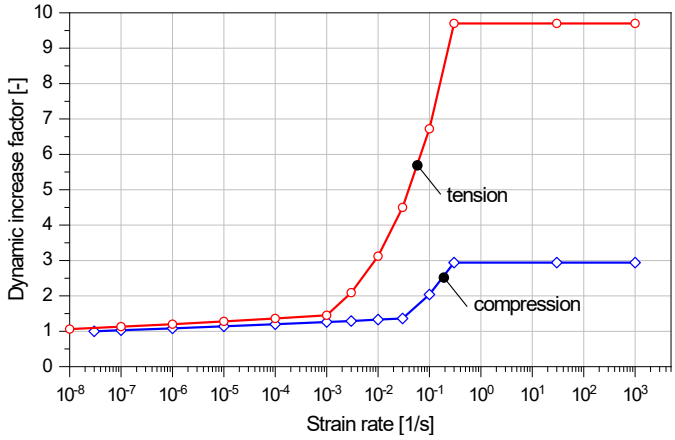


Figure 6 Strain-rate dependence utilized with the model.

$$\lambda = \int_0^{\bar{\varepsilon}^p} \frac{d\bar{\varepsilon}^p}{r_f (1 + p \,/\, r_f f_t)^{b1}}; \qquad \text{when } p \geq 0 \tag{17}$$

$$\lambda = \int_0^{\bar{\varepsilon}^p} \frac{d\bar{\varepsilon}^p}{r_f (1 + p \,/\, r_f f_t)^{b2}}; \qquad \text{when } p \leq 0 \tag{18}$$

$$d\bar{\varepsilon}^p = \sqrt{\frac{2}{3} \varepsilon_{ij}^p \varepsilon_{ij}^p} \tag{19}$$

The parameter r_f defines the dynamic increase factor (DIF) that takes strain-rate effect into account. Equations (17) and (18) are replaced in the recent version of the LS-Dyna with improved forms of Eqs. (20) and (21) see (Malvar, Crawford, and Morrill 2000).

$$\lambda = \int_0^{\bar{\varepsilon}^p} \frac{d\bar{\varepsilon}^p}{[1 + (s \,/\, 100)(r_f - 1)](1 + p \,/\, r_f f_t)^{b1}}; \qquad \text{for } p \geq 0 \tag{20}$$

$$\lambda = \int_0^{\bar{\varepsilon}^p} \frac{d\bar{\varepsilon}^p}{[1 + (s \,/\, 100)(r_f - 1)](1 + p \,/\, r_f f_t)^{b2}}; \qquad \text{for } p \leq 0 \tag{21}$$

In which the scaled damage, s, is user-defined and ranges from 0 to 100. When this parameter is set to 0, the strain-rate effect is eliminated in the damage calculation, and when set to 100, 100% of the strain-rate effect is used (Salamon and Harris 2014). In this work, the strain-rate effect is assumed to be active, and the K&C material model was enhanced with a pre-defined strain-rate curve of LS-Dyna User's Manual (LST- LIVERMORE SOFTWARE TECHNOLOGY, 2021) shown in Figure 6. Herein work, two input versions of the K&C were considered, including the automatic generation parameters option, i.e., the original and the modified versions. They will be referred to as K&C and modified K&C, respectively. A detailed description of the modified version is given in the following.

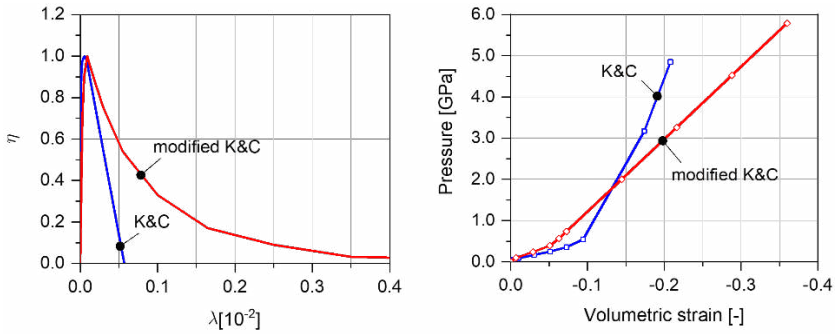
Table 2 Material specifications associated with each part.

Phase	Material parameter	value
Specimen (Cement-based) *MAT_072R3	Mass density [kg/m3]	1900
	Compressive strength [MPa]	40
	Tensile strength [MPa]	2.8
	Poisson ratio [-]	0.2
Incident bar (Aluminum) *MAT_001	Mass density [kg/m3]	2850
	Elastic modulus [GPa]	71
	Poisson ratio [-]	0.27
Transmitter bar (Brass) *MAT_001	Mass density [kg/m3]	8470
	Elastic modulus [GPa]	98
	Poisson's ratio [-]	0.3
Glue (Epoxy Resin)	Mass density [kg/m3]	1800
	Elastic modulus [GPa]	4.5

4.3.2 Calibration of K&C Material Model

One of the most significant uses of the K&C material model is the integrated capabilities of automatic parameters generation based on the uniaxial static compressive strength and the unit conversion balance RSIZE and UCF. This capability is very beneficial to users with limited experimental data in their hands. As discussed earlier, in the first step, the simulation was performed with the built-in auto-generation option, and then the model was extended with some modifications to improve the results.

There is a considerable effort addressed to calibrate and improve the K&C model; see, for instance, Markovich et al. (N. Markovich, Kochavi, and Ben-Dor 2009; Natalia Markovich, Kochavi, and Ben-Dor 2011) and Levi-Hevroni et al. (Levi-Hevroni et al. 2018). The calibration process suggested by (N. Markovich, Kochavi, and Ben-Dor 2009; Natalia Markovich, Kochavi, and Ben-Dor 2011) was found useful; therefore will be adopted. This improved calibration was carried out using a variety of experimental results of Attard and Setunge (Attard and Setunge 1996). The default parameters are first generated using the unconfirmed uniaxial compression strength, and then part of the automatically generated inputs are adjusted according to the specific requirements. The default generated parameters are stored together with the equation of state and the damage function parameters in the automatically generated output file named "*message*". The parameters can then be copied and modified from there. This calibration involves a number of parameters, namely the damage scaling in tension and compression, the equation of state, the damage function, and the tensile strength, see Eqs. (20) and (21).



(a) damage function **(b)** pressure-volumetric strain curve

Figure 7 Karagozian & Case concrete damage model.

An overview of the calibrated input parameters is listed in Table 3. The scaled damage and the equation-of-state for both K&C and modified K&C material models are compared in Figure 7.

Table 3 Calibrated equations of K&C

Material	b_2	s	f_t **[Gpa]**
K&C	1.35	100	0.0035
Modified K&C	1.10	0.5	0.0028

4.3.3 Material Model for Incident and Transmitter Bars

Brass and aluminum bars are assumed to behave as linear elastic materials for the analysis. Therefore, material type 1 (*MAT_001) in LS-Dyna was employed to specify their specifications. The mechanical parameters associated with each part of the simulation model are presented in Table 2 Material specifications associated with each Table 2.

5 RESULTS AND DISCUSSION

5.1 Dynamic Tensile Strength

An example of the simulated incident, reflected, and transmitted strain waves are compared along with the experimental ones in Figure 8. This comparison demonstrates that the LS-Dyna model is capable of capturing the behavior in an SNTB test.

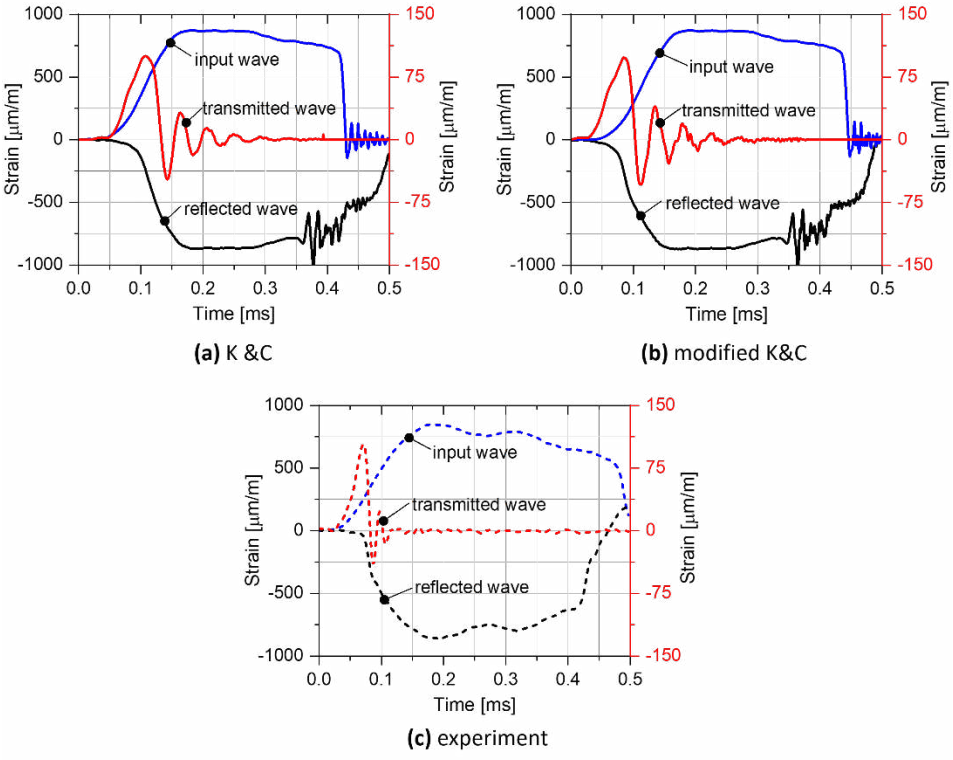


Figure 8 Input, reflected, and transmitted strain waves through time.

As mentioned earlier in Section 3, these signals are used together with Eq. (9) to evaluate the specimen's dynamic tensile strength based on the one-dimensional wave propagation (H. Kolsky 1949). The stress-time history measured from the experimental study and from the present simulations is presented in Figure 9 for comparison. As can be observed, the computation results exhibit good agreement, indicating the reliability of the K&C material formulation. According to Figure 9 and Table 4, it is clear that the directly computed tensile stress curves show considerable differences compared to the exact curves computed indirectly using Eq. (9). It should be noted that the directly computed stress is the average stress distribution along the radius of the specimen.

For the model analyzed using the built-in auto-generation of the K&C formulation, the indirectly computed strength peak $\sigma_s = 12.80$ MPa is slightly higher compared to the experimental strength $\sigma_s = 12.26$ MPa. A better agreement regarding both the peak tensile strength and the strain-softening behavior was achieved by adjusting a few material parameters $\sigma_s = 12.37$ MPa, see Figure 9(b). Therefore, it is undeniable that the modifications made to the K&C model obviously resulted in an enhanced agreement. However, the stain-softening behavior of the modified K&C model may still need further calibration to reproduce the recorded stress-time waves of the experimental study accurately.

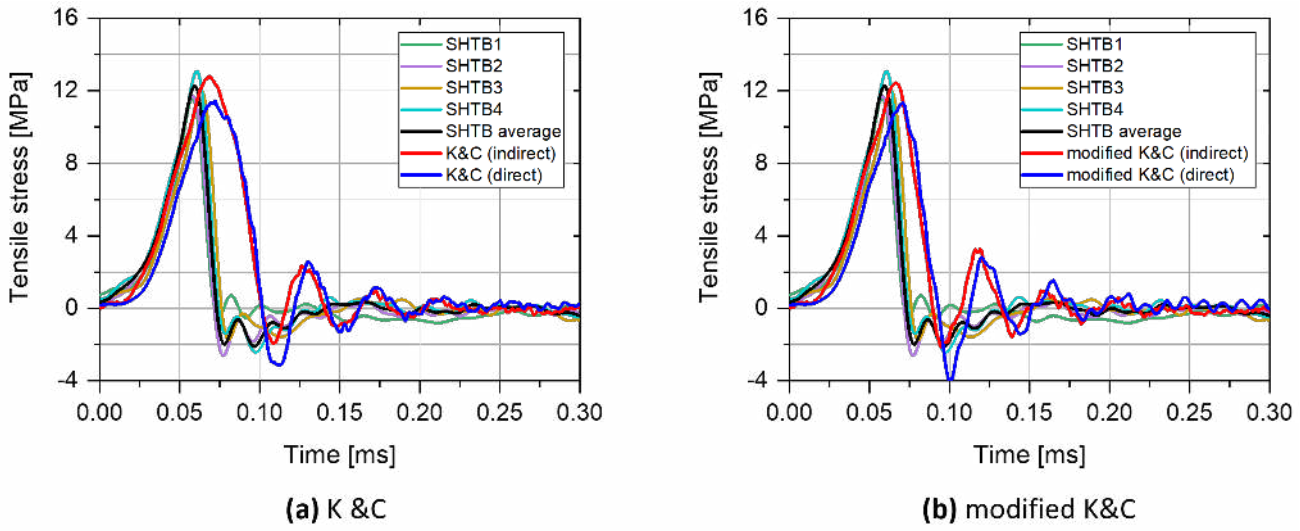


Figure 9 Comparison of the stress-time history.

For the stress-time profile shown in Figure 9, it should also be noted that there are time delays regarding the moment when the tensile stress reaches its peak value. The simulated peak stress is at 0.07 ms, whereas the averaged experimental is at 0.06 ms. This delay may be related to the strain-rate sensitivity of the K&C material model.

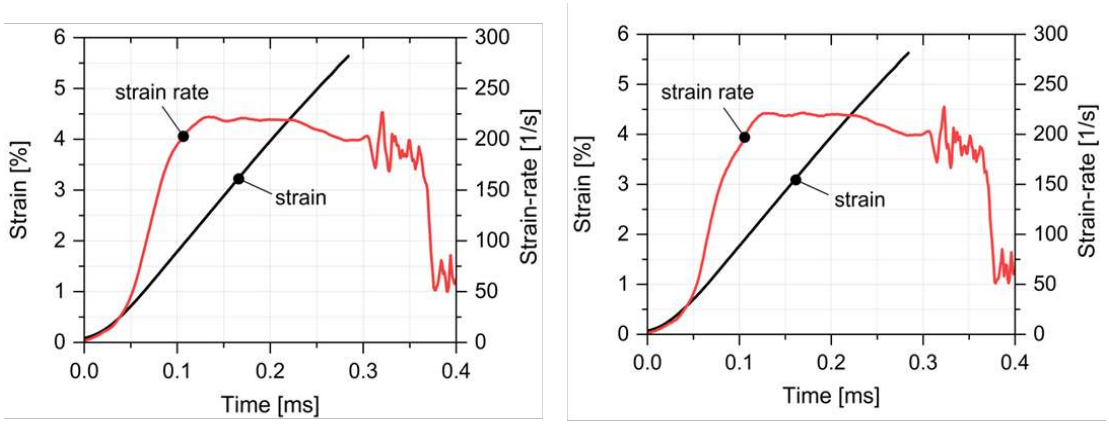
5.2 Strain and Strain-rate

The strain-rate profiles are presented in Figure 10 These curves were derived based on Eq. (11) as discussed earlier in Section 3. As can be seen, the strain-rate profile is not constant during the time due to the nature of the SHTB test. However, the computed strain-rate curves correspond well with the experimental ones.

Table 4 Results for computed and experimental strength.

Dynamic tensile strength σ_s [MPa]	Value
Experimental according to Eq. (9)	12.26
Simulation K&C (indirect) according to Eq. (9)	12.80
Simulation K&C (direct)	11.46
Simulation modified K&C (indirect) according to Eq. (9)	12.37
Simulation modified K&C (direct)	11.16

The strain-rate peak of about 223 and 225 s^{-1} was obtained from the analysis with the K&C and the modified K&C models, respectively, compared to the experimental of about 217 s^{-1}. The strain history computed according to Eq. (10) is also presented in Figure 10. If needed, the stress-time history illustrated in Figure 9 and the strain-time profiles of Figure 10 can be combined to yield the stress-strain behavior.



(a) K &C **(b)** modified K&C

Figure 10 Comparison of strain and strain-rate profiles.

6 CONCLUSIONS

In the present study, a numerical investigation on the high strain-rate response of the cement-based materials under tension was conducted. In particular, an split Hopkinson bar apparatus was simulated and analyzed in terms of strain signals, tensile strengths, strains, and strain-rates. The Karagozian & Case concrete damage material model has been successfully calibrated to reproduce the behavior of cement-based materials exposed to dynamic tensile loadings. Comparing the computational results with the available experimental data served to validate the numerical model. Satisfactory agreement was observed when comparing simulation and experimental data. The simulation models predicted the direct and indirect tensile strengths with good accuracy. The strain and strain-rate profiles were found to be in agreement with the experimental ones. In terms of softening behaviors captured by the K&C and the modified K&C, further calibrations might still be required to accurately reproduce the experimentally observed behavior.

Finite element analysis has been shown to be a helpful and valuable tool that provides insights into material details and has to be performed for certain materials whenever deep understanding and accurate results are important.

ACKNOWLEDGMENTS

The authors are deeply grateful for the support provided by the Sudanese Ministry of Higher Education and Scientific Research (MHESR) in conducting this study.

Author's Contributions: Conceptualization, A Babiker, E Abu-Elgasim, and M Mohammed; Methodology, A Babiker, E Abul-Elgasim and M Mohammed; Investigation, A Babiker, E Abu-Elagsim, and M Mohammed; Software A Babiker; Validation A Babiker E Abu-Elgasim, and M Mohammed; Visualization A Babiker; Writing - original draft, A Babiker, E Aabu-Elgasim and M Mohammed; Writing - review & editing, A Babiker.

Editor: Marcílio Alves

References

Attard, M. M., and S. Setunge. 1996. "Stress-Strain Relationship of Confined and Unconfined Concrete." *ACI Materials Journal* 93(5): 432–42.

Cadoni, E, and D Forni. 2016. "Experimental Analysis of the UHPFRCs Behavior under Tension at High Stress Rate." *Eur. Phys. J. Special Topics* 225: 253–64. https://link.springer.com/content/pdf/10.1140%2Fepjst%2Fe2016-02639-2.pdf (July 2, 2019).

Chen, Xudong, Shengxing Wu, and Jikai Zhou. 2014. "Experimental Study on Dynamic Tensile Strength of Cement Mortar Using Split Hopkinson Pressure Bar Technique." *Journal of Materials in Civil Engineering* 26(6): 1–10.

Cooper, R. H., and J. D. Campbell. 1967. "Testing of Materials at Medium Rates of Strain." *Journal of Mechanical Engineering Science* 9(4): 278–84.

Curosu, Iurie, Viktor Mechtcherine, Daniele Forni, and Ezio Cadoni. 2017. "Performance of Various Strain-Hardening Cement-Based Composites (SHCC) Subject to Uniaxial Impact Tensile Loading." *Cement and Concrete Research* 102(August): 16–28. http://dx.doi.org/10.1016/j.cemconres.2017.08.008.

Curosu, Iurie, Viktor Mechtcherine, and Oliver Millon. 2016. "Effect of Fiber Properties and Matrix Composition on the Tensile Behavior of Strain-Hardening Cement-Based Composites (SHCCs) Subject to Impact Loading." *Cement and Concrete Research* 82: 23–35. http://dx.doi.org/10.1016/j.cemconres.2015.12.008.

H. Kolsky. 1949. "An Investigation of the Mechanical Properties of Materials at Very High Rates of Loading." *Proceedings of the Physical Society. Section B*: 676–700.

Hao, Y. F., X. H. Zhang, and H. Hao. 2011. "Numerical Analysis of Concrete Material Properties at High Strain Rate under Direct Tension." *Procedia Engineering* 14(1): 336–43. http://dx.doi.org/10.1016/j.ijimpeng.2011.08.006.

Heravi, Ali A., Iurie Curosu, and Viktor Mechtcherine. 2020. "A Gravity-Driven Split Hopkinson Tension Bar for Investigating Quasi-Ductile and Strain-Hardening Cement-Based Composites under Tensile Impact Loading." *Cement and Concrete Composites* 105(April 2019): 103430. https://doi.org/10.1016/j.cemconcomp.2019.103430.

Levi-Hevroni, David et al. 2018. "Experimental and Numerical Investigation on the Dynamic Increase Factor of Tensile Strength in Concrete." *International Journal of Impact Engineering* 114(December 2017): 93–104. https://doi.org/10.1016/j.ijimpeng.2017.12.006.

Li, Weimin, and Jinyu Xu. 2009. "Impact Characterization of Basalt Fiber Reinforced Geopolymeric Concrete Using a 100-Mm-Diameter Split Hopkinson Pressure Bar." *Materials Science and Engineering: A* 513–514: 145–53. https://linkinghub.elsevier.com/retrieve/pii/S0921509309001890 (August 6, 2019).

LIVERMORE SOFTWARE TECHNOLOGY (LST), AN ANSYS COMPANY. 2021. II *LS-DYNA KEYWORD USER'S MANUAL - VOLUME II Material Models*. California: Livermore Software Tech. Comp. (LST), an Ansys Comp. www.lstc.com.

Malvar, LJ, JE Crawford, and KB Morrill. 2000. Karagozian and Case Structural Engineers, Technical Report TR-99-24.3 *K&C Concrete Material Model Release III-Automated Generation of Material Model Input*.

Malvar, LJ, JE Crawford, DA Simons, and JW Wesevich. 1995. "A Concrete Material Model for DYNA3D." *Engineering Mechanics*: 142–46.

Malvar, LJ, JE Crawford, JW Wesevich, and DA Simons. 1996. "A New Concrete Material Model for DYNA3D-Release II: Shear Dilation and Directional Rate Enhancements." *A Report to Defense Nuclear Agency under Contract No DNA001-91-C-0059*.

Markovich, N., E. Kochavi, and G. Ben-Dor. 2009. "Calibration of a Concrete Damage Material Model in LS-Dyna for a Wide Range of Concrete Strengths." *IWSRIB_2009_Haifa*.

Markovich, Natalia, Eytan Kochavi, and Gabi Ben-Dor. 2011. "An Improved Calibration of the Concrete Damage Model." *Finite Elements in Analysis and Design* 47(11): 1280–90. http://dx.doi.org/10.1016/j.finel.2011.05.008.

Nicholas, Theodore. 1981. "Tensile Testing of Materials at High Rates of Strain - An Experimental Technique Is Developed for Testing Materials at Strain Rates up to 103 s-1 in Tension Using a Modification of the Split Hopkinson Bar or Kolsky Apparatus." *Experimental Mechanics* 21(5): 177–85.

Ross, C. Allen, P. Y. Thompson, and J. W. Tedesco. 1989. "Split-Hopkinson Pressure-Bar Tests on Concrete and Mortar in Tension and Compression." *ACI Materials Journal* 86(5): 475–81.

Salamon, Jerzy, and David W. Harris. 2014. "Evaluation of Nonlinear Material Models in Concrete Dam Finite Element Analysis." (August): 87.

Staab, G H, and A Gilat. 1991. *A Direct-Tension Split Hopkinson Bar for High Strain-Rate Testing*. https://link.springer.com/content/pdf/10.1007%2FBF02326065.pdf (August 6, 2019).

Wang, Shasha, Min Hong Zhang, and Ser Tong Quek. 2012. "Mechanical Behavior of Fiber-Reinforced High-Strength Concrete Subjected to High Strain-Rate Compressive Loading." *Construction and Building Materials* 31: 1–11. http://dx.doi.org/10.1016/j.conbuildmat.2011.12.083.